The USP14–NLRC5 pathway inhibits titanium particle–induced osteolysis in mice by suppressing NF-κB and PI3K/AKT activities

Received for publication, December 29, 2019, and in revised form, March 31, 2020 Published, Papers in Press, April 9, 2020, DOI 10.1074/jbc.RA119.012495

Guibin Fang[1], **Yuan Fu**[1], **Shixun Li, Junxiong Qiu, Manyuan Kuang, Sipeng Lin, Changchuan Li, and Yue Ding**[2]

From the Department of Orthopaedic Surgery, Sun Yat-Sen Memorial Hospital, Sun Yat-Sen University, Guangzhou 510120, China

Edited by Peter Cresswell

Total hip arthroplasty (THA) is a widely-used surgical intervention for treating patients with end-stage degenerative and inflammatory osteoarthropathy. However, wear particles from the artificial titanium joint can induce osteolysis, limiting the long-term survivorship of THA. Monocyte/macrophage lineage cells are the key players in the response to wear particles, and the proinflammatory NF-κB and phosphoinositide 3-kinase (PI3K)–AKT Ser/Thr kinase (AKT)-signaling pathways have been shown to be the most important contributors to wear particle–induced osteolysis. In contrast, ubiquitin-specific protease 14 (USP14) specifically removes the polyubiquitin chains from the nucleotide-binding and oligomerization domain (NOD)-like receptor family Caspase recruitment domain (CARD)–containing 5 (NLRC5) and thereby enhances the NLRC5-mediated inhibition of NF-κB signaling. In this study, we aimed to clarify the role of the USP14–NLRC5 pathway in wear particle–induced osteolysis *in vitro* and *in vivo*. We found that NLRC5 or USP14 overexpression inhibits titanium particle–induced proinflammatory tumor necrosis factor α (TNFα) production and NF-κB pathway activation, and it also decreases M1 macrophage polarization and PI3K/AKT pathway activation. Of note, NLRC5 and USP14 overexpression attenuated titanium particle–induced cranial osteolysis in mice. In conclusion, the findings of our study indicate that the USP14–NLRC5 pathway inhibits titanium particle–induced osteolysis by suppressing the NF-κB and PI3K/AKT pathways both *in vitro* and *in vivo*.

Total hip arthroplasty (THA)[3] is a successful and widely-used surgical procedure for the treatment of end-stage degenerative and inflammatory osteoarthropathy. However, hip prosthesis only has an in-service life of 15–25 years, and nearly all of the patients need to receive revision surgery (1). According to a complication-based analysis using worldwide arthroplasty registers, the most common cause for revision in THA was aseptic loosening (55.2%) (2). In China, a retrospective study conducted on 405 consecutive patients who underwent revision hip arthroplasty found that prosthesis loosening was the most common cause for revision hip arthroplasty (69.14%) (3). It has been reported that wear particles from the artificial joint are the triggering cause of periprosthetic osteolysis and the consequent aseptic loosening (4). Unfortunately, there is no effective nonsurgical treatment to prevent and cure this complication currently. Therefore, it is necessary to explore new strategies for reducing wear particle–induced periprosthetic osteolysis in order to prolong the longevity of the artificial joint.

Monocyte/macrophage lineage cells play a significant role in immunology, tissue homeostasis, disease pathogenesis, and inflammation. Macrophages are the key players in the response to wear particles from prostheses (5). Macrophages, upon activation by wear particles, release a series of proinflammatory cytokines such as tumor necrosis factor-α (TNFα), interleukin-6 (IL-6), and interleukin-1β (IL-1β), which recruit and activate osteoclast precursors and trigger inflammatory bone resorption. Subsequently, mature osteoclast-mediated bone resorption leads to periprosthetic osteolysis and long-term aseptic loosening (6, 7). Macrophage activation in osteolysis may lead to macrophage polarization (8). After exposure to different stimuli, the resting macrophages (M0) are capable of polarizing to two specific phenotypes with "classically-" and "alternatively-" activated macrophages, representing proinflammatory M1 and anti-inflammatory M2 macrophages (9). Wear particles have been proved to activate the macrophages that induced an M1 macrophage phenotype promoting local secretion of inflammatory cytokines (10). M1 macrophage polarization is associated with high levels of these cytokines, so it is tempting to ascribe M1 macrophages as cells promoting osteoclastogenesis, although the M2 macrophages would inhibit this process (11). In addition, numerous studies *in vivo*

This work was supported by the Key Laboratory of Malignant Tumor Molecular Mechanism and Translational Medicine of Guangzhou Bureau of Science and Information Technology, National Natural Science Fund Grant 81672186, and Natural Science Foundation of Guangdong Province Grant 2017B030311016. The authors declare that they have no conflicts of interest with the contents of this article.

This article contains Figs. S1 and S2.

[1] Both authors contributed equally to this work.

[2] To whom correspondence should be addressed. E-mail: dingyue@mail.sysu.edu.cn.

[3] The abbreviations used are: THA, total hip arthroplasty; LPS, lipopolysaccharide; NC, negative control; GAPDH, glyceraldehyde-3-phosphate dehydrogenase; ROI, region of interest; BV/TV, bone volume/tissue volume; BMD, bone mineral density; PI3K, phosphoinositide 3-kinase; RANK, receptor activator of NF-κB; RANKL, receptor activator of NF-κB ligand; NOD, nucleotide-binding and oligomerization domain; NLR, nucleotide-binding domain and leucine-rich repeat; TLR, Toll-like receptor; PRR, pattern recognition receptor; TNFα, tumor necrosis factor-α; IL, interleukin; AL, aseptic loosening; FHN, femoral head necrosis; IS, immunoreactivity score; DAB, diaminobenzidine; EGFP, enhanced GFP; ELISA, enzyme-linked immunosorbent assay; BLI, bioluminescence imaging; iNOS, inducible nitric-oxide synthase; CARD, Caspase recruitment domain.

and *in vitro* have indicated that the inhibition of the macrophage polarization to the M1 phenotype might be served as novel therapeutic strategies for periprosthetic osteolysis (6, 12). Although it is commonly believed that macrophages are the key cells in the response to wear particles associated with periprosthetic osteolysis, how the macrophages were activated and polarized is poorly understood.

Inflammatory reactions associated with wear particles in macrophages are mediated by several important signaling pathways, the most important of which involves the NF-κB and phosphoinositide 3-kinase/Akt (PI3K/Akt) pathways. NF-κB activation is essential for macrophage recruitment and maturation, inducing the production of pro-inflammatory cytokines and chemokines such as TNFα, IL-6, and IL-1β (13). Moreover, NF-κB activation contributes to osteoclast differentiation and maturation via binding of RANKL and osteoclast-associated RANK (14). A number of researchers have reported that repressing NF-κB–signaling pathway activation could attenuate wear debris–induced osteolysis (15–17). Our previous study has shown that the PI3K/Akt pathway plays a positive role in the regulation of activating macrophages by wear particles. The inhibition of the PI3K/Akt pathway reduces TNFα production in the macrophage response to wear particles *in vitro* (18, 19). Furthermore, TNFα promoted osteoclast precursor cell differentiation through the PI3K/Akt-signaling pathway (20). Also, the PI3K/Akt pathway has been identified as one of the numerous signaling pathways essential for promoting macrophage M1 polarization over the years (21). Therefore, a potential therapeutic strategy to prevent implant loosening is to suppress NF-κB- and PI3K/Akt-signaling pathways, and our previous studies have explored them. However, the effects are not totally satisfactory and are far from clinical applications. Undoubtedly, it is necessary to explore new regulators of these signaling pathways.

The NOD-like receptor family CARD domain containing 5 (NLRC5) is the largest member of the nucleotide-binding domain and leucine-rich repeat (NLR) family, involved in various physiological processes, such as inflammation, innate immunity, and diabetic nephropathy (22). Several studies have identified NLRC5 as a negative regulator that blocks IKKα and IKKβ, two central components of the NF-κB–signaling pathways, and has important roles in homeostatic control of innate immunity (23, 24). NLRC5 negatively regulates TLR2-mediated allergic airway inflammation via the NF-κB pathway (25). Besides, knockdown of NLRC5 *in vitro* attenuates renal I/R injury *in vitro* through the activation of the PI3K/Akt-signaling pathway (26). Recently, it has been reported that ubiquitin-specific protease 14 (USP14) specifically removes the polyubiquitin chains from NLRC5 to enhance NLRC5-mediated inhibition of NF-κB signaling (27). USP14 is one of three proteasome-associated deubiquitinating enzymes that remove ubiquitin from proteasomal substrates prior to their degradation. However, very little is known about the role of USP14/NLRC5 in the process of wear particles activating macrophages and triggering periprosthetic osteolysis and aseptic loosening.

This study therefore investigates the effect of USP14/NLRC5 to regulate the inflammatory response of macrophages and periprosthetic osteolysis due to wear particles.

Results

TNFα was highly expressed while NLRC5 and USP14 expression decreased in synovial membrane around the prosthesis in patients with aseptic loosening

The brown color in Fig. 1*A* showed the staining intensity of the interest protein expressed in cytoplasm. TNFα was barely detected in synovial tissues of patients with femoral head necrosis but was highly expressed in the synovial membrane around the prosthesis in patients with aseptic loosening. In contrast, there is a lower expression of NLRC5 and USP14 in the patients with aseptic loosening compared with patients with femoral head necrosis (Fig. 1*A*). The average immunoreactivity score (IS) of TNFα in AL group was 1.57 ± 0.21, significantly higher than that in FHN patients (0.17 ± 0.12, $p < 0.05$), similar to the tendency of IL-6 (1.33 ± 0.21 *versus* 0.15 ± 0.06). Meanwhile, the average IS of NLRC5 significantly decreased in the AL group compared with FHN group (0.28 ± 0.10 *versus* 1.13 ± 0.15, $p < 0.05$). A similar tendency was found in USP14 (0.22 ± 0.13 *versus* 1.05 ± 0.13, $p < 0.05$) (Fig. 1*B*).

TNFα, NLRC5, and USP14 mRNA levels were up-regulated in J77A.1 cells after more than 1 h of Ti stimulation in vitro, whereas the protein expression levels of NLRC5 and USP14 reversed

To investigate the expression change of TNFα, NLRC5, and USP14 at different levels in macrophages after stimulation by Ti particles, we performed real-time PCR, Western blotting, and ELISA with J774A.1 cells and the culture supernatants. The mRNA expression of TNFα in macrophages was significantly up-regulated after the stimulation of Ti particles at every time point ($p < 0.05$). Besides, mRNA expressions of NLRC5 and USP14 decreased after 1 h of Ti stimulation and kept up-regulating when stimulated for more than 1 h ($p < 0.05$) (Fig. 2*A*). ELISA results showed that the concentration of TNFα-secreted protein in the culture supernatants increased continuously when stimulated by Ti particles (Fig. 2*B*). In contrast, protein levels of NLRC5 and USP14 decreased in J774A.1 cells when treated with Ti particles and LPS for 24 h, whereas the ubiquitination level of NLRC5 by Ti particles and LPS treatment was enhanced at 1 h after stimulation (Fig. 2*C*).

Higher expression of proinflammatory cytokine was observed in USP14/NLRC5 down-regulated J774a.1 cells and knockdown of USP14 enhanced the activation of NF-κB signaling pathway due to Ti stimulation

NF-κB–signaling pathway and downstream proinflammatory cytokines play an important role in wear particle–induced periprosthetic osteolysis. Thus, we investigated the effect of USP14 and NLRC5 on the NF-κB pathway and TNFα and in J774A.1 cells stimulated by Ti particles. We stimulated the USP14/NLRC5-knockdown J774a.1 cells and the negative control cells with the Ti particles, and then we performed real-time PCR and ELISA to examine the expression of TNFα. An increased mRNA expression of TNFα was observed in USP14/NLRC5-knockdown J774a.1 cells compared with the negative

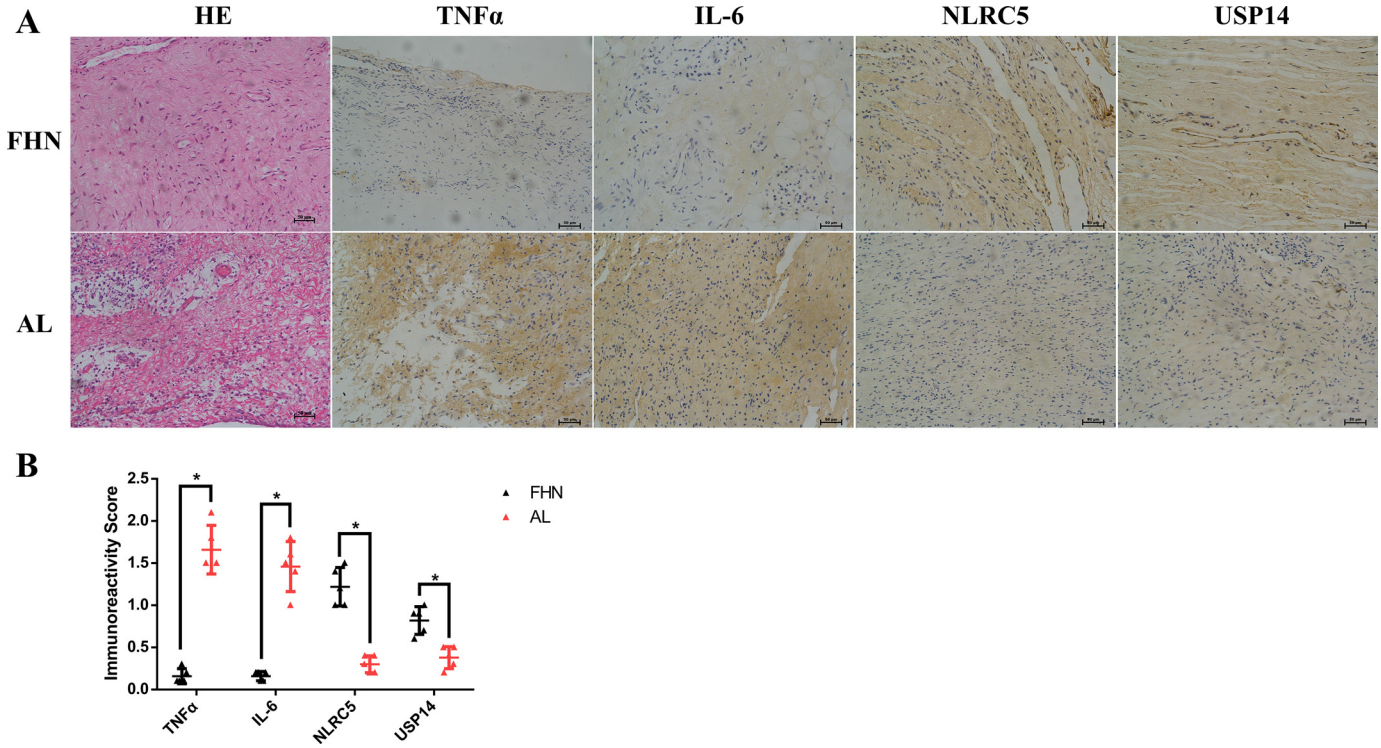

Figure 1. Expression of TNFα, IL-6, NLRC5, and USP14 in hip synovial membrane of patients with femoral head necrosis and aseptic loosening. *A,* immunohistochemical staining of TNFα, IL-6, NLRC5, and USP14 from AL and FHN patients' hip synovial membrane. *B,* immunoreactivity score of TNFα, IL-6, NLRC5, and USP14 from AL and FHN patients' hip synovial membrane. *, $p < 0.05$.

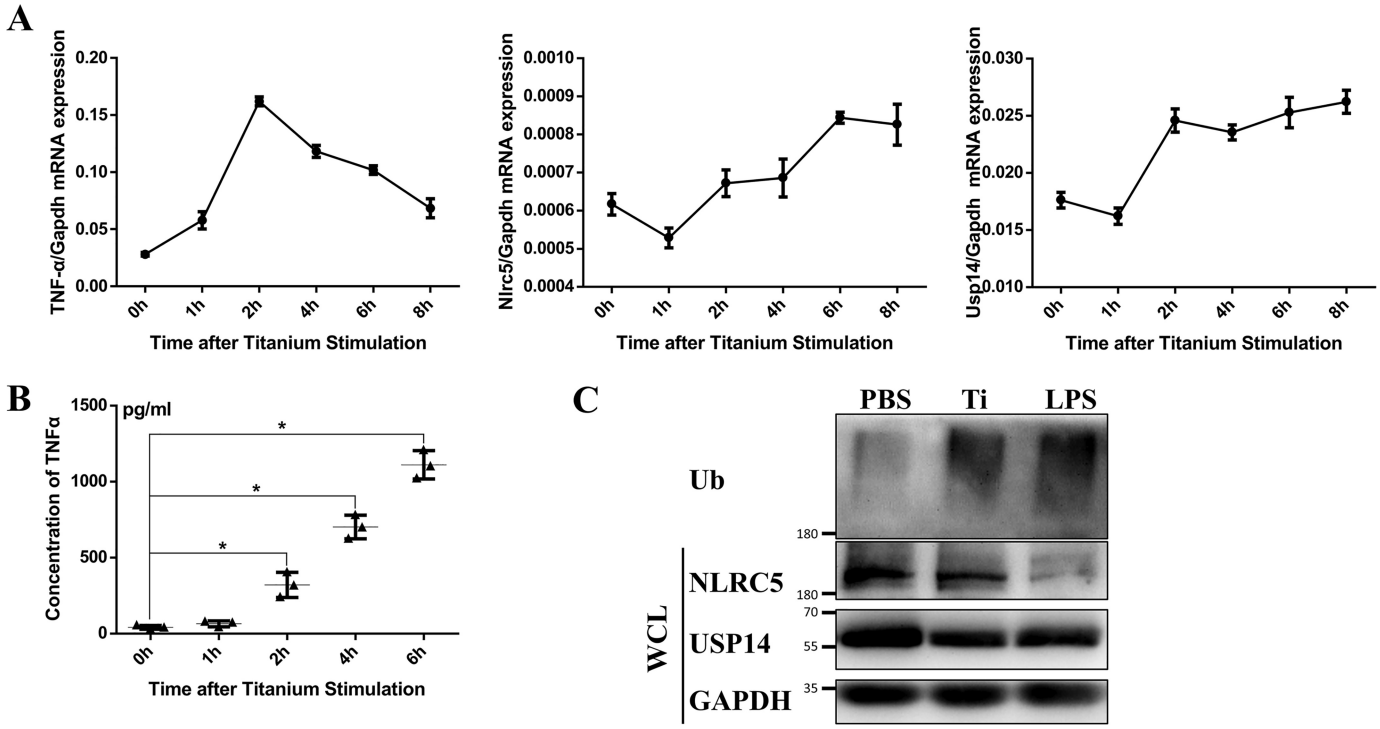

Figure 2. mRNA and protein expression levels of TNFα, NLRC5, and USP14 in J774A.1 cells stimulated by Ti particles for different times. *A,* mRNA expression levels of TNFα, NLRC5, and USP14 at each time point after stimulation of Ti particles (0, 1, 2, 4, 6, and 8 h). *B,* secreted TNFα protein expression at each time point after stimulation (0, 1, 2, 4, and 6 h), detected by ELISA. *, $p < 0.05$. *C,* protein expression of TNFα, NLRC5, and USP14 after stimulation for 24 h and the ubiquitination (*Ub*) level of NLRC5 by Ti particles and LPS treatment for 1 h. *WCL*, whole-cell lysate.

control cells at each time points after stimulation ($p < 0.05$) (Fig. 3*A*). ELISA results showed the similar increase in secreted protein of TNFα in USP14/NLRC5-knockdown J774a.1 cells compared with the negative control cells after stimulation ($p < 0.05$) (Fig. 3*B*). Immunofluorescent staining and Western blotting were performed to explore the effect of USP14 and NLRC5

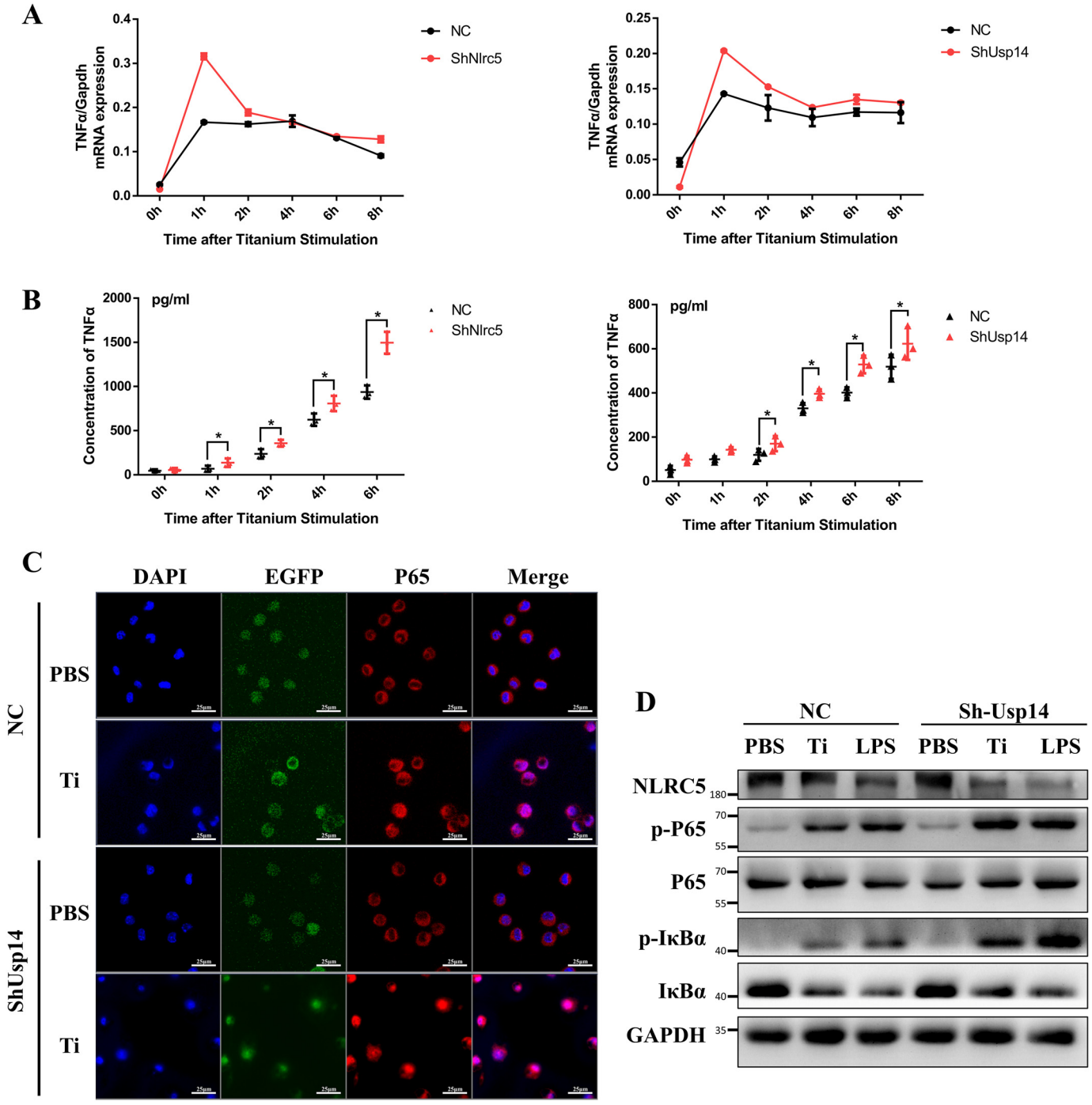

Figure 3. Expression of TNFα and NF-κB pathway in USP14 or NLRC5-knockdown J774A.1 macrophage compares with negative control cells after titanium stimulation. *A,* higher mRNA expression of TNFα in USP14/NLRC5-knockdown J774A.1 cells compared with negative control cells after titanium stimulation. *B,* more secreted TNFα protein was detected in USP14/NLRC5-knockdown J774A.1 cells compared with negative control cells at every time point after titanium stimulation. *, $p < 0.05$. *C,* P65 was observed with more translocation into the nuclei of USP14-knockdown J774a.1 cells than those of control cells after Ti stimulation. *D,* protein expression of phospho-IκBα and phospho-P65 in the NF-κB pathway and NLRC5 in USP14-knockdown J774a.1 cells and negative control cells after titanium and LPS stimulation. *DAPI,* 4,6-diamidino-2-phenylindole.

on the NF-κB–signaling pathway. As the immunofluorescent staining results showed, P65, a transcription factor of the NF-κB family, was observed with more translocation into nuclei of USP14-knockdown J774a.1 cells than those of control cells after Ti stimulation for 1 h (Fig. 3*C*). Quantitative analysis of fluorescence imaging confirmed that the ratio of P65 fluorescence value at the nucleus/cytoplasm in USP14-knockdown J774A.1 cells is higher than that in negative control cells (Fig. S1*A*), representing the enhanced activation of NF-κB–signaling pathway. What's more, Western blotting showed that the protein expression of phospho-IκBα and phospho-P65 was up-regulated after Ti and LPS stimulation, which was enhanced by the knockdown of USP14. Meanwhile, NLRC5 protein in USP14-knockdown J774A.1 cells decreased after Ti and LPS stimulation compared with NC cells, but no change was observed between the groups without stimulation (Fig. 3*D*).

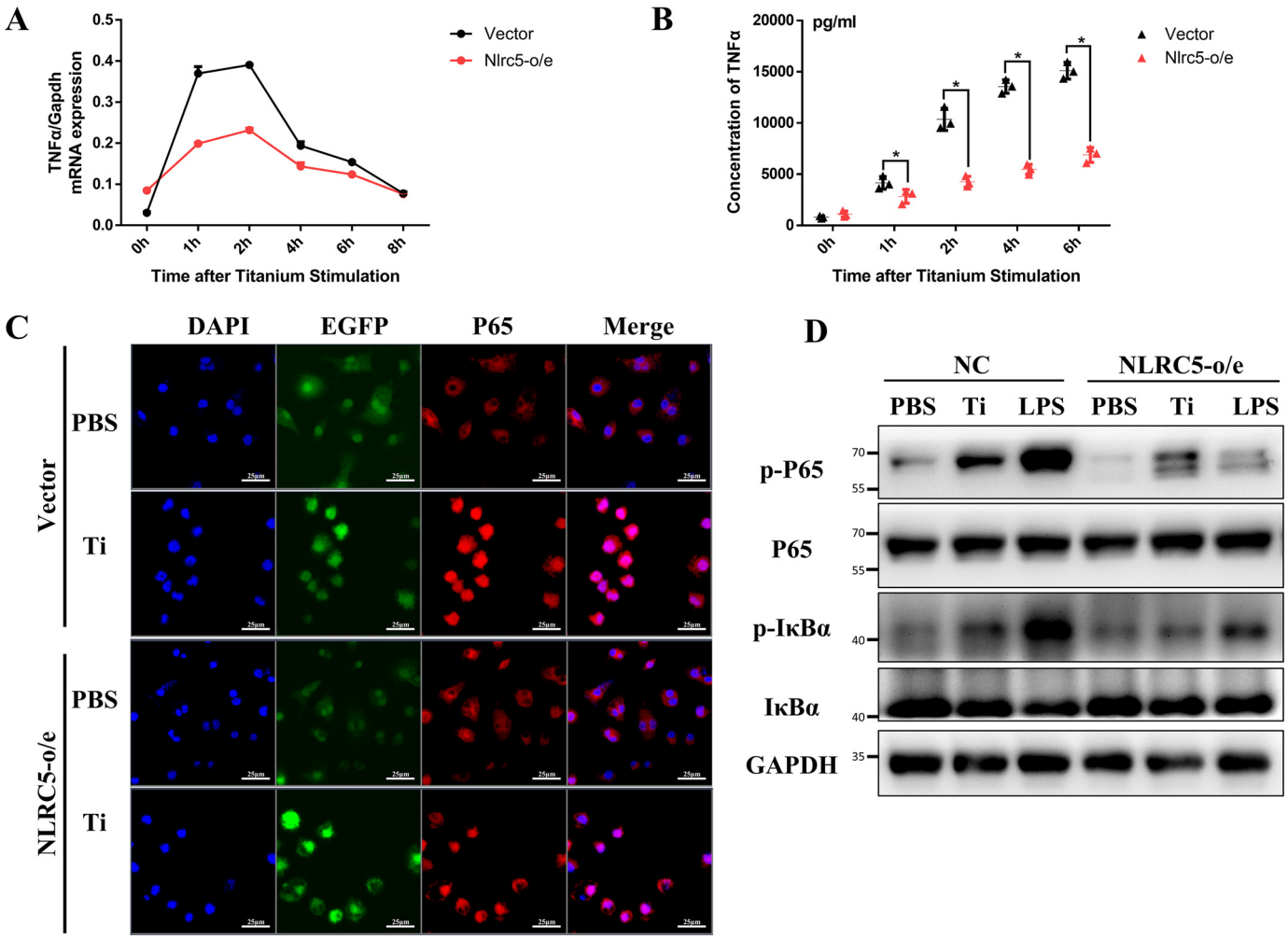

Figure 4. Expression of TNFα and NF-κB pathway in NLRC5-overexpressed J774A.1 cells compared with normal cells after titanium stimulation. *A,* overexpression of NLRC5 significantly suppressed the mRNA expression of TNFα after titanium stimulation. *B,* lower concentration of secreted TNFα protein was detected in NLRC5-overexpressed J774A.1 cells compared with normal cells at every time point after titanium stimulation. *, $p < 0.05$. *C,* P65 was observed with less translocation into the nuclei of NLRC5 overexpressed J774A.1 cells than those of normal cells after titanium stimulation. *D,* protein expression of phospho-IκBα and phospho-P65 in NLRC5-overexpressed J774a.1 cells and normal cells after titanium and LPS stimulation.

Overexpression of NLRC5 and USP14 attenuated the expression of TNFα and activation of NF-κB–signaling pathway

To further elucidate the effect of USP14 and NLRC5 on the NF-κB pathway and TNFα and in J774A.1 cells stimulated by Ti particles, we transfected USP14/NLRC5-expressing vector into J774A.1 cells to overexpress USP14 and NLRC5. Real-time PCR and ELISA were performed to examine the expression of TNFα after stimulation by Ti particles. As shown in Figs. 4*A* and 5*A*, overexpression of NLRC5 or USP14 significantly suppressed the mRNA expression of TNFα ($p < 0.05$). ELISA results showed that both USP14 and NLRC5 overexpression significantly attenuated the increase in secreted protein of TNFα ($p < 0.05$) (Figs. 4*B* and 5*B*). Immunofluorescent staining results showed that NLRC5 or USP14 overexpression reduced the translocation of P65 into the nuclei after Ti stimulation (Figs. 4*C* and 5*C*), which was confirmed by the quantitative analysis of the fluorescence image (Fig. S1, *B* and *C*). Apparently, Western blotting results showed that overexpression of NLRC5 or USP14 suppressed the up-regulation of protein expression of phospho-IκBα and phospho-P65 after Ti and LPS stimulation, confirming the effect of NLRC5 and USP14 on the NF-κB–signaling pathway (Figs. 4*D* and 5*D*). Besides, the protein level of NLRC5 in USP14-overexpressed cells was higher than that of normal cells, while its ubiquitinated level decreased in USP14-overexpressed J774A.1 cells compared with normal cells after Ti and LPS stimulations (Fig. 4*D*).

Overexpression of NLRC5 and USP14 attenuated the M1 polarization of macrophages induced by Ti particles

After stimulating by Ti particles for 24 h, the different macrophage phenotypes of J774a.1 cells were analyzed by flow cytometry. The macrophages were identified by F4/80 and the M1-specific marker, iNOS. Representative dot plots of the different experimental groups are displayed in Fig. 6*A*. The flow cytometry results showed that the Ti stimulation caused an increase in the percentage of iNOS-positive cells in all groups (0.233 ± 0.08% *versus* 10.287 ± 0.878%, 0.360 ± 0.205% *versus* 7.007 ± 0.818%, and 0.537 ± 0.293% *versus* 2.350 ± 1.000%), and overexpression of NLRC5 and USP14 attenuated this M1 polarization of macrophages (Fig. 6*B*). To further explore the mechanisms of how USP14 and NLRC5 attenuated the M1

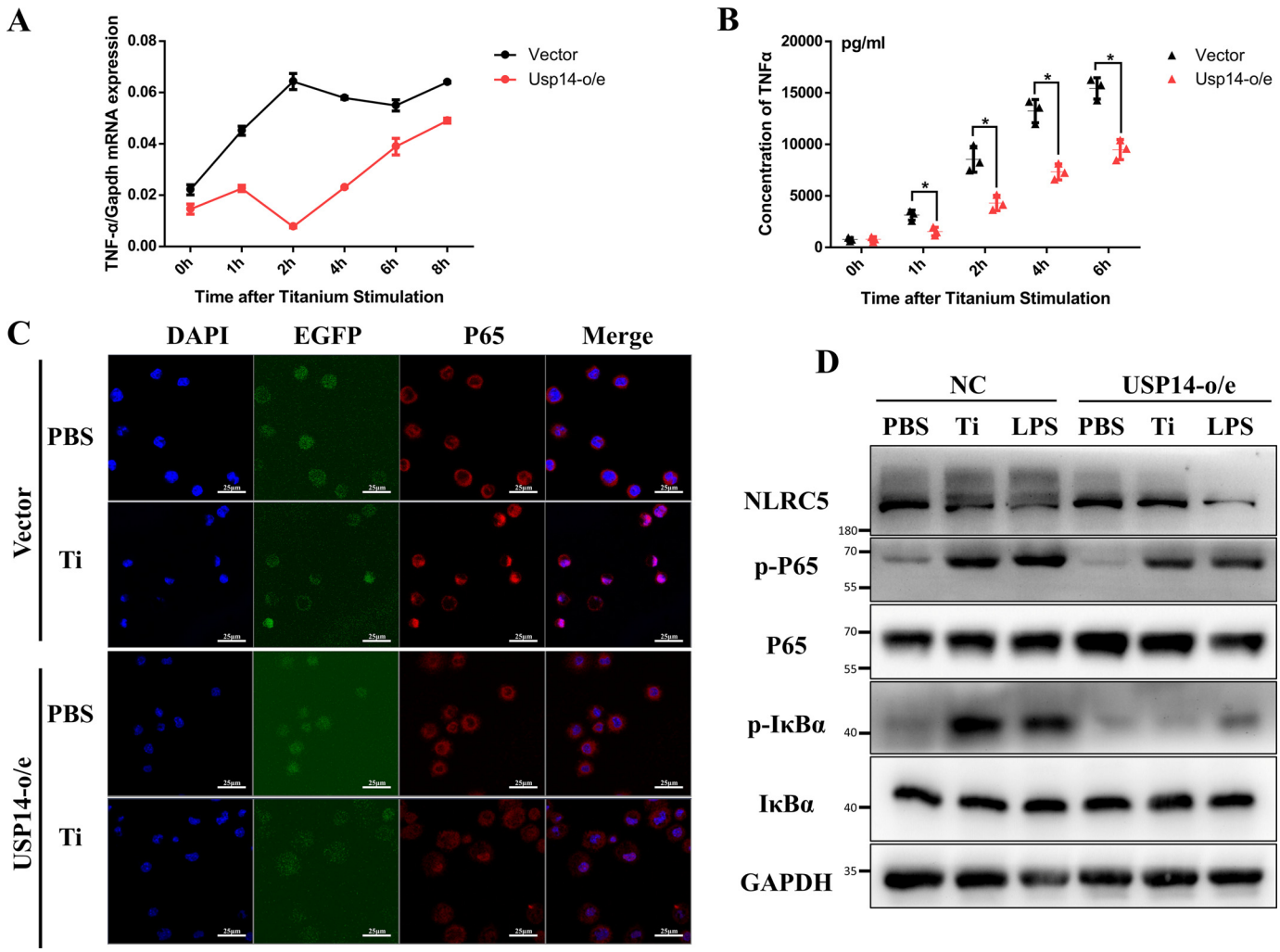

Figure 5. Expression of TNFα and NF-κB pathway in USP14-overexpressed J774A.1 cells compared with normal cells after titanium stimulation. *A,* overexpression of USP14 significantly suppressed the mRNA expression of TNFα after titanium stimulation. *B,* lower concentration of secreted TNFα protein was detected in USP14-overexpressed J774A.1 cells compared with normal cells at every time point after titanium stimulation. *, $p < 0.05$. *C,* P65 was observed with less translocation into the nuclei of USP14-overexpressed J774A.1 cells than those of normal cells after titanium stimulation. *D,* protein expression of phospho-IκBα, phospho-P65, and NLRC5 as well as its ubiquitination level in USP14-overexpressed J774a.1 cells and normal cells after titanium and LPS stimulation.

polarization of macrophages induced by Ti particles, Western blotting was carried out to observe the effect of USP14 and NLRC5 on the PI3K/Akt-signaling pathway 30 min after Ti stimulation. As shown in Fig. 6*C*, PI3K and Akt protein expression kept still while phospho-PI3K and phospho-Akt protein expressions were up-regulated after Ti stimulation, which was attenuated by NLRC5 and USP14 overexpression.

Overexpression of NLRC5 and USP14 prevented the cranial osteolysis of mice induced by wear particles in vivo

The mouse model of cranial osteolysis induced by Ti particles was performed, and the local macrophage recruitment on the mid-line sagittal suture of the calvarium was investigated by BLI following the injection of the J774A.1 reporter macrophage expressing luciferase. From day 1 to day 7, bioluminescence was observed on the vertical images of mice injected with J774A.1 reporter cells that were respectively designed as NLRC5 and USP14-overexpressed and normal vector cells, indicating the continuous macrophage recruitment induced by Ti particles and the J774A.1 cells with genetic manipulation reactions to Ti particles (Fig. 7*A*). 7 days later, the crania of all the mice were harvested and performed with micro-CT scanning. 3-Dimensional reconstruction of the mouse crania showed an area of osteolysis around the cranial sutures in the mice treated with titanium particles compared with the sham group, which was alleviated by the overexpression of NLRC5 or USP14 (Fig. 7*B*). Bone volume/tissue volume (BV/TV) and bone mineral density (BMD) of a 1 × 3-mm region of interest (ROI) around the cranial suture were evaluated by micro-CT. Quantitative analysis in Table 1 showed a significant decrease in Ti-treated groups compared with a sham group in BV/TV ($p < 0.05$) and BMD ($p < 0.05$). Ti particle–induced bone loss was significantly attenuated in the NLRC5/USP14-overexpressed group ($p < 0.05$, Fig. 7*C*).

Overexpression of NLRC5 and USP14 inhibited the expression of proinflammatory cytokine and formation of osteoclasts in vivo

Immunohistochemistry assay of mouse calvaria showed that the proinflammatory cytokines TNFα and IL-6 were highly

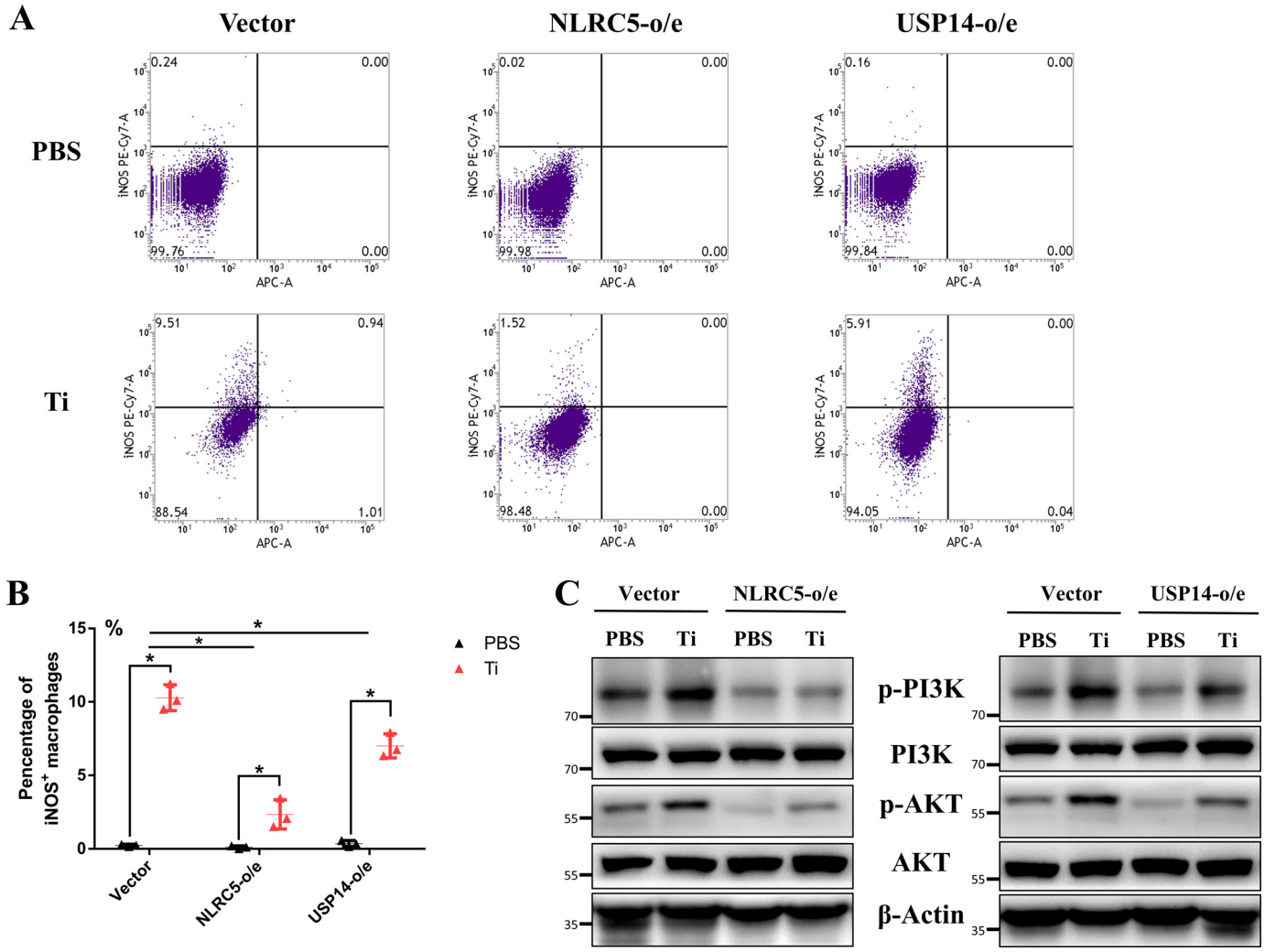

Figure 6. Flow cytometry of macrophage polarization and PI3K/Akt pathway in each group of J774A.1 cells after stimulation by Ti particles. *A* and *B*, M1 polarization of macrophages detected by flow cytometry in USP14/NLRC5-overexpressed J774A.1 cells compared with those transfected with negative control vector after Ti stimulation. *, $p < 0.05$. *C*, protein expression of PI3K/Akt pathway in USP14/NLRC5-overexpressed J774A.1 cells compared with negative control cells.

expressed in the Ti-treated groups compared with the sham group. But within the Ti-treated groups, TNFα and IL-6 expression levels in the NLRC5 and USP14 overexpression groups were lower than those of the normal cells group. Trap$^+$ cell numbers per field of the normal group (34.00 ± 6.40 cells), the NLRC5-overexpressed group (23.80 ± 3.70 cells), and the USP14-overexpressed group (24.80 ± 5.26 cells) were significantly more than that of Sham group (12.20 ± 3.11 cells, $p <$ 0.05 respectively). Meanwhile, the Trap$^+$ cells in NLRC5/USP14-overexpressed groups were lower than those in normal group (Fig. 8*A*). Counting of Trap$^+$ cell numbers confirmed the above conclusion (Fig. 8*B*).

Discussion

The long-term survivorship of THA is limited by wear particle–induced osteolysis, in which the monocyte/macrophage lineage cells play a pivotal role. The biotoxicity, biocompatibility, and mechanics properties have been greatly renovated with the regeneration of prosthesis materials, but the aseptic loosening caused by wear particles still remain unsolved (1). Upon activation by wear particles, macrophages release a series of proinflammatory cytokine-like TNFα, IL-6, and IL-1β, which induce the recruitment of macrophage and trigger the activation of osteoclast precursors (4, 5). It has been reported that the interaction between TNFα and RANKL promotes osteoclast activity associated with wear debris (14). Advances have identified the activated RANKL/RANK–receptor complex as a fundamental factor that promotes physiological osteoclast formation. Previous studies had proved that in this process the NF-κB and PI3K/Akt pathway plays a positive role in the regulation of activating macrophages by wear particles and the production of TNFα. Therefore, modulation of the macrophage activation state and production of proinflammatory cytokines through the NF-κB and PI3K/Akt pathway would appear to be an available strategy for attenuating wear particle–induced osteolysis (15–19).

The innate immune response is elicited through the detection of pathogen-associated molecular patterns, which depends on several classes of pattern recognition receptors (PRRs), including mainly the Toll-like receptors (TLRs) and the NOD-

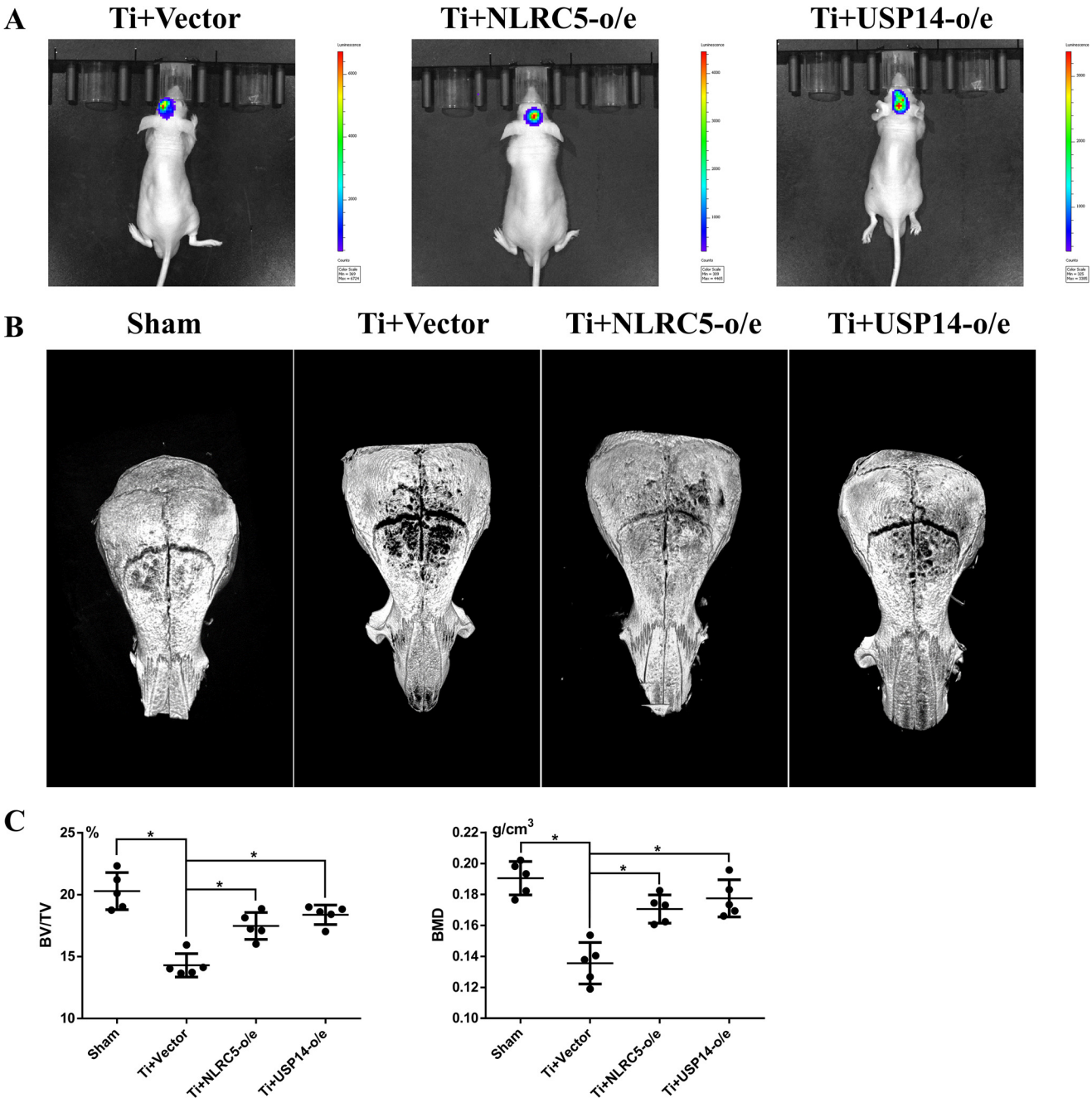

Figure 7. Local injection of NLRC5/USP14-overexpressed J774A.1 cells alleviated the cranial osteolysis of mice induced by Ti particles *in vivo*. *A,* from day 1 to day 7, bioluminescence was observed focused on the mid-line sagittal suture of the calvaria on the vertical images of mice injected with J774A.1 reporter cells expressing luciferase. *B,* 3-dimensional reconstruction of the mouse crania micro-CT showed an area of osteolysis around the cranial sutures in the mice treated with titanium particles compared with the sham group, and the osteolysis was alleviated by the overexpression of NLRC5 and USP14. *C,* BV/TV and BMD of a 1 × 3-mm ROI around the cranial suture evaluated by micro-CT. *, $p < 0.05$.

Table 1
BV/TV and BMD of each group of mice. o/e , overexpressed

	Sham (mean ± S.D.)	Ti$^+$ vector (mean ± S.D.)	Ti$^+$ NLRC5-o/e (mean ± S.D.)	Ti$^+$ USP14-o/e (mean ± S.D.)
BV/TV (%)	20.29 ± 1.50	14.30 ± 0.94	17.48 ± 1.09	18.38 ± 0.79
BMD (g/cm^3)	0.190 ± 0.011	0.136 ± 0.013	0.171 ± 0.009	0.177 ± 0.012

like receptors (NLRs) (28). In our previous studies, a large number of macrophages with abundant TLRs (including TLR2 and TLR4) and NLRs have been found in the synovial membrane samples from patients with aseptic loosening, indicating that macrophages might recognize the wear particles through PRRs (29). Activation of most TLRs leads to a series of downstream signaling events that culminate in NF-κB activation. NLRs represent a large family of intracellular PRRs that are characterized

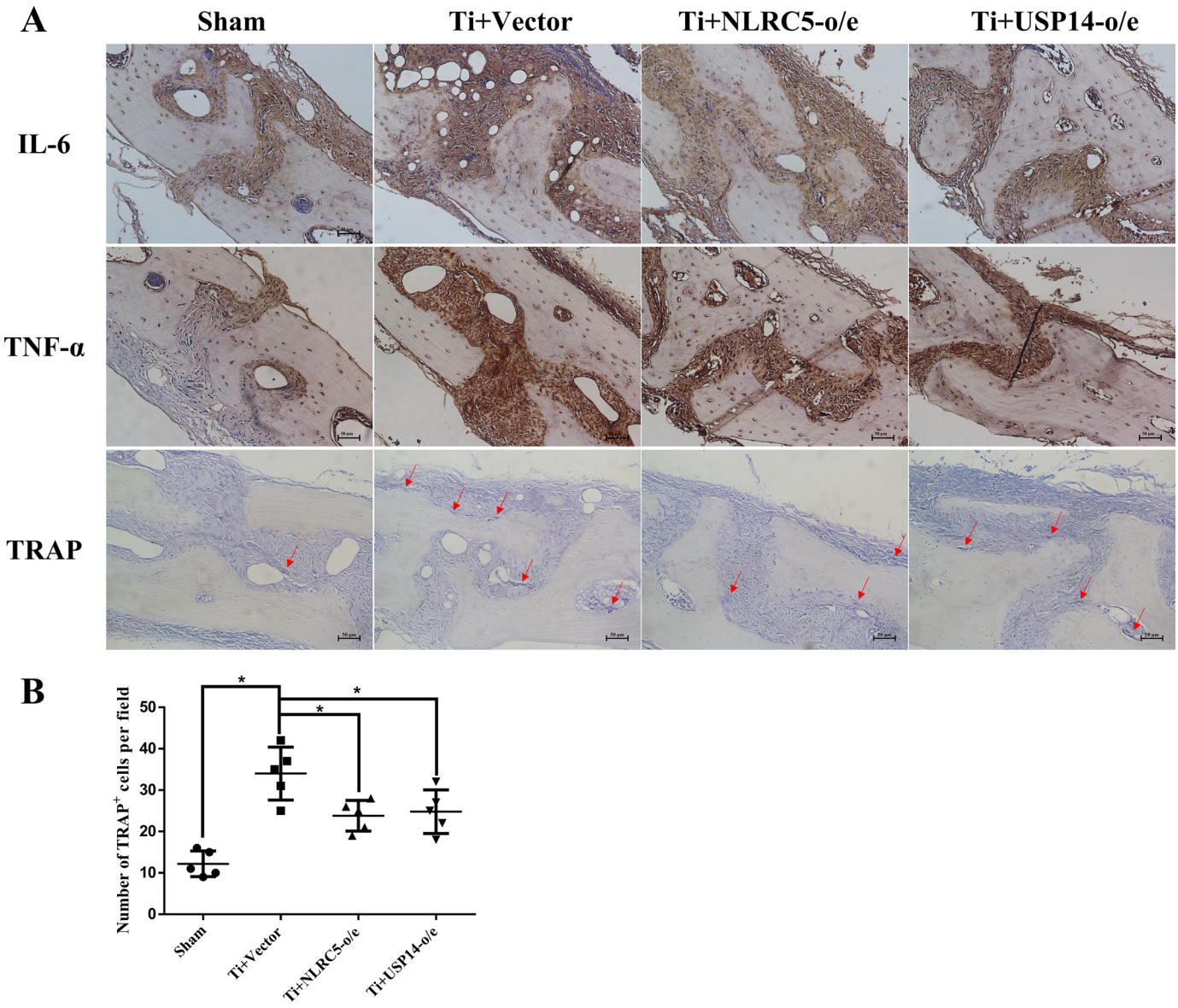

Figure 8. Expression of IL-6, TNFα, and TRAP of mouse calvarial sutures in different treatment groups. *A,* immunohistochemical staining of IL-6, TNFα, and TRAP of mouse calvarial sutures in different treatment groups. *B,* Trap$^+$ counting of cell numbers in the mouse calvarial sutures in the different treatment groups. *, $p < 0.05$.

by a NOD and a leucine-rich repeat region and are involved in the activation of diverse inflammatory signaling pathways (30). The NOD-like receptor family CARD domain containing 5 (NLRC5) is the largest member of NLR family involved in various physiological processes, such as inflammation, innate immunity, and diabetic nephropathy.

NLRC5 has been identified as a negative regulator that blocks two central components of the NF-κB–signaling pathways induced by TLR ligands and important role in homeostatic control of innate immunity. It strongly inhibits NF-κB– dependent responses by interacting with IKKα and IKKβ and blocking their phosphorylation (23). NLRC5 negatively regulates inflammatory response via a TLR2/NF-κB pathway in macrophages and also participates in TLR2-mediated allergic airway inflammation (25). Meanwhile, enhanced TLR-induced NF-κB signaling was detected in NLRC5-deficient mice (24). What's more, it is reported that knockdown of NLRC5 *in vitro* enhanced the activation of the PI3K/Akt-signaling pathway (26).

Furthermore, research by Meng *et al.* (27) found that ubiquitination editing of NLRC5 determined NLRC5–IKKβ interaction dynamics and enhanced the activation of NF-κB signaling. Protein ubiquitination is an exceptionally-flexible post-translational modification that regulates a wide variety of signaling pathways. USP14 is one of three proteasome-associated deubiquitinating enzymes that remove ubiquitin from proteasomal substrates prior to their degradation (31). USP14 specifically removes the polyubiquitin chains from NLRC5 to enhance the interaction between NLRC5 and IKK-β, thus inhibiting NF-κB activation in an NLRC5-dependent coherent feedforward loop manner (27). Given that NLRC5 is involved in many biological processes and functions as a negative regulator of NF-κB- and PI3K/Akt-signaling pathways, we hypothesized

that NLRC5 negatively regulates the titanium particle-induced osteolysis *in vitro* and *in vivo*, which is enhanced by USP14. As mentioned above, numerous studies, including our previous ones, had focused on the roles of TLRs, NOD2, as well as NLRP3 in wear particle–induced osteolysis, but few studies had reported the role of USP14/NLRC5 in aseptic loosening. Besides, recent studies on NLRC5 mostly put their concentration on the relevance of NLRC5 in homeostasis and activity of CD8 T cells and natural killer lymphocytes in controlling infection and cancer (32–34). Therefore, our investigation into the roles of USP4/NLRC5 of macrophages in wear particle–induced osteolysis might provide an innovative therapeutic strategy for attenuating aseptic loosening.

In this study, TNFα were observed highly expressed, whereas NLRC5 and USP14 expression decreased in synovial membrane around the prosthesis in the patients with aseptic loosening. NLRC5 expression decreased due to the robust ubiquitination upon Ti stimulation, similar to the effect of LPS challenge (27). To further explore how NLRC5 and USP14 function in aseptic loosening, we carried out the following *in vitro* studies. As described before, titanium particles ranging from 0.2 to 1.2 μm were proved to induced more secretion of proinflammatory cytokine and thus were chosen in this study to stimulate the maximal biological effect (29). Likewise, the mRNA expression and secreted protein levels in the culture supernatants of TNFα were up-regulated in J774A.1 cells after stimulation with titanium particles. Interestingly, the mRNA expression level of NLRC5 and USP14 decreased after 1 h of Ti stimulation and was kept up-regulated when stimulated for more than 2 h, just contrary to their decreasing trend of protein expression levels *in vivo* and *in vitro*. A possible explanation for this might be that the mRNA expression level of NLRC5 and USP14 increased due to a negative feedback regulation to the reducing protein level. These preliminary results indicated that NLRC5 and USP14 might be involved in the process of wear particle–induced immunoreaction.

To further identify the role of NLRC5 and USP14 in wear particle–induced osteolysis, we generated the stably-transfected NLRC5 and USP14-knockdown J774A.1 cells with lentivirus and stimulated each group of cells with Ti particles. The expression of proinflammatory cytokine TNFα in NLRC5 and USP14-knockdown J774A.1 cells was respectively found higher than that in the NC group both in mRNA and secreted protein levels. Meanwhile, protein expression of NF-κB pathway was up-regulated in USP14-knockdown J774A.1 cells after Ti stimulation, indicating that the activation NF-κB pathway was enhanced in USP14-knockdown cells. This was confirmed by the immunofluorescent results, which showed that more P65 translocated into the nuclei of USP14-knockdown J774a.1 cells compared with NC cells after Ti stimulation. Also, the protein level of NLRC5 decreased in USP14-knockdown cells, which might be caused by the enhanced ubiquitination and increasing degradation of NLRC5, as USP14-mediated deubiquitination was attenuated after USP14 was down-regulated. These results strongly suggested that USP14/NLRC5 played a negative role in the inflammatory response induced by Ti particles and was consistent with the previous studies that found that NLRC5 negatively regulated the NF-κB–signaling pathway and USP14 shaped NLRC5 function and modulated NF-κB activation switch (23, 25, 27).

Previous studies had verified the negative roles of NLRC5 and USP14 through the knockdown or knockout of the gene (24, 27), but no evidence had confirmed their attenuating effect on inflammation through the overexpression of NLRC5 and USP14. Thus, we respectively generated the NLRC5- and USP14-overexpressed J774A.1 cells by transfecting them with specific lentivirus so as to redouble the evidence of their negative effect on Ti particle–induced osteolysis. Further analysis showed that the mRNA and secreted protein levels of TNFα were down-regulated by the overexpression of NLRC5 and USP14, respectively. Similarly, the activation of the NF-κB pathway was observed to be inhibited by Western blotting and immunofluorescent staining, confirming the negative roles of NLRC5 and USP14 in regulating Ti particle–induced immunoreaction. Therefore, the level of ubiquitinated NLRC5 decreased in USP14-overexpressed J774A.1 cells compared with normal cells, which might be the cause of increasing protein levels of NLRC5 in USP14-overexpressed cells compared with normal cells after Ti and LPS stimulations because USP14-mediated deubiquitination on NLRC5 was enhanced. Collectively, we hypothesized that NLRC5 negatively participated in Ti particle–induced inflammatory response by inhibiting the NF-κB pathway, and USP14 enhanced this function of NLRC5 through a deubiquitination mechanism.

In the process of periprosthetic osteolysis, macrophage polarization toward the M1 phenotype also functions as a significant factor, which promotes local secretion of inflammatory cytokines and bone destruction (8, 10, 11). In general, macrophage activation and polarization to the M1 phenotype recruit and activate osteoclast precursors and trigger inflammatory bone resorption, thus leading to periprosthetic osteolysis, limiting the long-term survivorship of artificial joint. In this study, the M1 subtype of macrophages was identified by specific marker iNOS through flow cytometry. Related analysis showed that the Ti stimulation caused an increase in the percentage of M1 macrophages, which was attenuated by the overexpression of NLRC5 and USP14. However, the mechanisms of how USP14/NLRC5 inhibits macrophage polarization toward M1 phenotypes remain unclear. The PI3K/Akt pathway is one of the numerous signaling pathways that have been identified to be essential for promoting macrophage polarization over the years. LPS induce the activation of M1 macrophages via TLR-mediated PI3K/Akt pathway (21, 35). Research by Qi *et al.* (36) verified that the level of macrophage M1 polarization could be inhibited by restraining the activation of the PI3K/Akt pathway by hesperidin in rheumatoid arthritis (RA). Knockdown of NLRC5 *in vitro* enhanced the activation of the PI3K/Akt-signaling pathway, indicating that NLRC5 could inhibit the activation of PI3K/Akt-signaling pathway (26). Furthermore, it has been proved in our previous study (18) that inhibition of the PI3K/Akt pathway reduced TNFα production in the cellular response to wear particles *in vitro*. Consistent with these previous results, this study observed that the PI3K/Akt pathway was activated after Ti stimulation, which could be inhibited by the overexpression of NLRC5 and USP14. Therefore, we hypothesize that NLRC5 might attenuate the M1 polarization of macro-

phages induced by Ti particles by inhibiting the PI3K/Akt-signaling pathway *in vitro* and that USP14 shapes NLRC5 function and modulates PI3K/Akt activation.

Further investigation is required to verify the negative role of USP14/NLRC5 in wear particle–induced osteolysis *in vivo* for developing an innovative therapeutic strategy for attenuating aseptic loosening. In generating the mouse model of cranial osteolysis, a gelatin sponge was used to maintain the suspension of titanium particles and keep them releasing slowly to make sure that titanium particles keep stimulating the interested area for 1 week. In our previous study, NOD2-knockdown lentivirus was injected locally to observe the effect on the cranial osteolysis in the mouse model (37). However, neither the efficiency of transfection nor the distribution of lentivirus could be observed and quantified after the injection of lentivirus. Therefore, murine reporter macrophages modified into different groups were injected at the mid-line sagittal suture of the calvaria to simulate the local infusion of macrophages in the presence of Ti particle stimuli. The BLI *in vivo* confirmed that macrophages of each group were recruited to the area of inflammation for 7 days. Similar to the results *in vitro*, the local injection of NLRC5- or USP14-overexpressed J774A.1 cells attenuated the cranial osteolysis induced by Ti particles, with significantly higher BV/TV and BMD compared with normal vector cells (Table 1). Immunohistochemistry assay of mouse calvaria confirmed the above results as the overexpression of NLRC5 and USP14 suppressed IL-6 and TNFα expression and osteoclastogenesis.

Several limitations in this study should be noted. J774A.1 cells were used as the reporter cells to verify the recruitment of macrophages to the area of particle-induced inflammation. J774A.1 cells are immortal macrophages derived from leukemia, which may cause cachexia of the mice 2–3 weeks after cell injection due to excessive proliferation. Indeed, further studies using the disease pattern animal model with NLRC5 or USP14 gene overexpression may be useful to further investigate the direct effects of NLRC5 and USP14 on cranial osteolysis of mice as induced by Ti particles (29). However, Zhao and co-workers (38) reported that USP14 overexpression in lung epithelial cells increased cytokine release. A study by Li *et al.* (39) also revealed that USP14 aggravated the dedifferentiation effect of IL-1β on chondrocytes, which might be bad for cartilage regeneration after destruction by osteoarthritis. Therefore, it is hard to determine whether there will be other issues if genome-wide overexpression of NLRC5 and USP14 is performed in mice. Further investigations such as monocyte/macrophage-specific NLRC5 and USP14 overexpression are required for our future studies.

Experimental procedures

Clinical synovium specimen collection and immunohistochemistry assay

Synovium specimens from sites of osteolysis were taken from seven patients undergoing revision surgery with the diagnosis of aseptic hip prosthesis loosening. Control samples of synovial tissue were obtained from 13 patients undertaking primary THA with the diagnosis of FHN. Synovial tissue was obtained from around the prosthesis in the AL group and from the hip in the control group. All the patients were informed and agreed to this study. This study was approved by the Ethics Committee of Sun Yat-sen University, Sun Yat-sen Memorial Hospital, in accordance with its guidelines (2017, Ethics Record no. 26).

Tissue samples were fixed immediately in 4% formalin fixative for paraffin embedding. Paraffin blocks were stored at room temperature. 3.0-μm serial sections were cut using a microtome and mounted on glass slides. Subsequently, the sections were deparaffinized through xylene immersion after heating for 2 h, rehydrating by graded ethanol, and subsequently permeabilizing for 20 min with 0.1% (v/v) Triton X-100, followed by treating with 0.1% trypsin for 30 min at 37 °C for antigen retrieval. After blocking in 5% BSA for 30 min at 37 °C, the sections were hatched with anti-human TNFα mouse mAb (1:100 diluted, Abcam), anti-human USP14 polyclonal antibody (1:100 dilution, 14517-1-AP, Proteintech Group), and anti-human NLRC5 polyclonal antibody (1:200 dilution, ab117624, Abcam) at 37 °C for 2 h, followed by cultivation with horseradish peroxidase–conjugated secondary antibody (Zhongshanjinqiao Biotechnology, China) for 30 min at 37 °C. Diaminobenzidine (DAB) was used as chromogenic agent, and hematoxylin was used for the second stain. Finally, the samples were washed by water, dried, and mounted with Neutral balsam and then observed with a biomicroscope (DM2000, Leica, German).

Bresalier's semiquantitative scoring system (40) was carried out by two independent observers in a blinded fashion to evaluate 10 views of each immunostained section. Briefly, both staining intensity (0 for no staining; 1 for weak staining; 2 for moderate staining; 3 for strong staining) and the percentage of stained cells were identified. Scores for staining intensity and percentage positivity of cells were then multiplied to generate the IS for each case: $\Sigma(0 \times F0 + 1 \times F1 + 2 \times F2 + 3 \times F3)$.

Particles

Commercial Ti particles diluted with pure water were purchased from Alfa Aesar (Ward Hill, MA) and then filtered by isopore filter membranes (Millipore) in a filter holder, so as to obtain the Ti particles with a diameter of 0.2–1.2 μm (average diameter: 0.82 $\pm$ 0.12 μm) (29). The Ti particles on the filter membranes were washed with 70% ethanol, which was evaporated from the Ti particle mixture and weighted after drying. The particles were sterilized with ethylene oxide and then resuspended in sterile PBS at a concentration to 4×10^8 mm^3/ml and kept in a −80 °C freezer. The particles were tested negative for endotoxin (<0.01 EU/ml) by Limulus amebocyte lysate assay (QCl-1000; BioWhittaker, Walkersville, MD).

Cell culture

Monocyte/macrophage lineage cell J774A.1 (ATCC, Manassas, VA) was cultured in Dulbecco's modified Eagle's medium (Gibco) containing 10% fetal bovine serum (Gibco) and 100 units/ml penicillin and 100 μg/ml streptomycin (Sigma) and incubated in a humidified incubator (Thermo Fisher Scientific, Waltham, MA) at the temperature of 37 °C with 5% CO_2. For analysis, J774A.1 cells were seeded in six-well plates (Costar, Cambridge, MA) at a concentration of 2×10^5 cells/ml and

Table 2
Sequences of USP14 shRNA and NLRC5–shRNA

No.	Gene	Gene sequence (5′ to 3′)
1	sh-Usp14–289	5′-AACCUCCAAUGGUGUUCATT-3′
2	sh-Usp14–1176	5′-CUACCUGCUUACUUAACUTT-3′
3	sh-Usp14–1255	5′-AUGUUAAGUUUCCUCUUATT-3′
4	sh-Nlrc5	5′-CCAGAACTCAGGAAATTTAACTTGA-3′
5	Negative control	5′-UUCUCCGAACGUGUCACGUTT-3′
6	GAPDH	5′-CACUCAAGAUUGUCAGCAATT-3′

then incubated overnight. Cell counter (Countstar, BioTech, Urbana, IL) was used to perform cell count and assess their viability (more than 98% in all trials).

Particle stimulation

24 h after seeding in culture plates, cells were treated with or without Ti particles at a final concentration of 100:1 (particle volume (μm^3)/cell number). LPS 100 ng/liter was used as positive control and PBS was used as negative control (NC). After addition of Ti particles or LPS, the culture plates including NC cells were gently shaken for 5 min to distribute Ti particles or LPS evenly. At different time points, the supernatants and TRIzol reagent (TaKaRa, Shiga, Japan)-treated cells were harvested. Cells were lysed in RIPA buffer supplemented with protease and phosphatase inhibitor mixture and harvested for Western blot analysis of NF-κB and PI3K/Akt signaling pathway 60 and 30 min respectively, after different stimulation.

shRNA synthesis, plasmid construction, and lentivirus transfection

Three USP14 shRNA sequences and negative control sequences (Table 2) were designed and synthesized by GenePharma Co. Ltd. (Suzhou, China). The corresponding lentivirus expression vector was hU6–MCS–ubiquitin–EGFP–IRES–puromycin (GenePharma Co. Ltd.). J774A.1 cells were cultured in six-well plates at a quantity of 2×10^5 cells per well and transfected with 200 μl of lentivirus per well with 2 μg/ml Polybrene for 24 h, according to the manufacturer's instructions. Cells were treated with puromycin (1 μg/ml) (InvivoGen, San Diego, CA) to produce stably-transfected cells (NC-shRNA, USP14-shRNA#1–3) for further experiments. The full-length USP14 cDNA was synthesized by RT-PCR from murine macrophages. Then USP14 cDNA was subcloned into the CN550–pLOV–EF1a–PuroRCMV–EGFP–2A-3-FLAG plasmid (Obio Technology Co. Ltd., Shanghai, China). The USP14 plasmid and corresponding empty vector were transfected into J774A.1 cells using Lipofectamine 2000 reagent (Invitrogen) following the manufacturer's protocol. Stably-transfected cells (vector, USP14-overexpressed) were selected by using puromycin (1 μg/ml) (InvivoGen). Down-regulation and overexpression of USP14 were confirmed by quantitative real-time PCR and Western blot analysis Fig. S2.

Oligonucleotides were synthesized for the generation of an annealing shRNA targeting the sequence of NLRC5 (VB181101-1227taq, Cyagen BioSciences, Inc.) as described by Cui *et al.* (23) The corresponding lentivirus expression vector was hU6–MCS–Nlrc5–EGFP–IRES–puromycin (Cyagen BioSciences, Inc.). The guide RNA (gRNA), which can specifically bind the regulatory region and up-regulate the expression of NLRC5, together with dCas9/VP64 and MS2/P65/HSF1 were designed and constructed by Cyagen BioSciences, Inc. The corresponding lentivirus packaging was performed by Cyagen BioSciences, Inc. J774A.1 cells were infected with the filtered lentivirus in the presence of 2 μg/ml Polybrene. Stably transfected cells (NC, sh-NLRC5, vector, NLRC5-overexpressed) were selected by using puromycin (1 μg/ml) (InvivoGen). Down-regulation and overexpression of NLRC5 were also confirmed by quantitative real-time PCR and Western blot analysis Fig. S2.

Quantitative real-time PCR

Total RNA was extracted from J774A.1 cells using TRIzol reagent (TaKaRa, Shiga, Japan), and the concentration of total RNA was measured by NanoDrop technology (Thermo Fisher Scientific). The first-strand cDNA was synthesized from 1 μg of total RNA using Primescript RT MasterMix (TaKaRa, Shiga, Japan) following the manufacturer's instructions. The CFX Connect (Bio-Rad) was used in quantitative real-time PCR to measure the mRNA levels. We analyzed the relative quantity of mRNA using the $2^{-\Delta\Delta Ct}$ method and the internal control to GAPDH. The primers of target genes are shown in Table 3.

TNFα measurement by instant ELISA

After culture for the indicated time points (1, 2, 4, 6, and 8 h), the supernatants of cells were harvested and centrifuged to remove cellular debris. Aliquots were stored at −20 °C for TNFα measurement by mouse TNFα Instant ELISA kit (eBioscience, Vienna, Austria), which was carried out according to the manufacturer's instructions. All assays were performed in duplicate.

Western blotting

Total proteins were extracted from J774A.1 cells using RIPA lysis buffer (Cell Signaling Technology). The protein concentrations in the supernatants were examined with a BCA protein assay kit (Invitrogen). A total of 30 μg of proteins were separated by 10% SDS-PAGE and transferred onto polyvinylidene difluoride membranes (Millipore Corp., Billerica, MA). After blocking with 5% (w/v) BSA (Beyotime Institute of Biotechnology) in Tris-buffered saline (TBS) with 0.1% (w/v) Tween 20, the membranes were reacted with primary antibodies and gently shaken at 4 °C overnight against the following: IκBα (1:1000 dilution, Cell Signaling Technology); phospho-IκBα (1:1000 dilution, Cell Signaling Technology); NF-κB p65 (1:1000 dilution, Cell Signaling Technology); phospho-NF-κB p65 (1:1000 dilution, Cell Signaling Technology); Akt (pan) (1:1000 dilution, Cell Signaling Technology); phospho-Akt (1:2000 dilution, Cell Signaling Technology); PI3K (1:1000 dilution, Cell Signaling Technology); phospho-PI3K (1:1000 dilution, Cell Signaling Technology); GAPDH (1:1000 dilution, Cell Signaling Technology); and β-actin (1:1000 dilution, Cell Signaling Technology). Bound antibodies were then detected with a horseradish peroxidase–linked secondary antibody (Cell Signaling Technology). Immunoreactive bands were imaged with a Bio-Imaging system (SYNGENE) based on the manufacturer's instructions.

Immunofluorescent staining and confocal microscopy

J774A.1 cells of each group were seeded with 0.4×10^6 cells per well in six-well culture plates with three 1 × 1-cm pieces of

Table 3
Primers of mRNAs used in this study

Gene	Forward (5′ to 3′)	Reverse (5′ to 3′)
USP14	ATGCCACTCTACTCTGTTACAGT	AACACCATTGGAGGTTCATCAG
NLRC5	GTGCCAAACGTCCTTTTCAGA	AGTGAGGAGTAAGCCATGCTC
TNFα	CCTGTAGCCCACGTCGTAG	GGGAGTAGACAAGGTACAACCC
GAPDH	TGTGTCCGTCGTGGATCTGA	TTGCTGTTGAAGTCGCAGGAG

glass in each well and incubated overnight. 1 h after stimulation, the cells were washed three times with PBS and then fixed in 4% paraformaldehyde for 15 min. Subsequently, the cells were treated with 0.1% Triton X-100, a 15-min gentle shake for permeabilization, followed by three washes with PBS. Then the cells were blocked in PBS containing 1% BSA for 30 min, followed by incubation with 50 μl of primary antibodies diluted 1:50 in 1% BSA in PBS overnight at 4 °C. Cells were washed three times with PBS followed by incubation with secondary antibodies goat anti-rabbit IgG (H+L) labeled by red fluorescence (EarthOxDylight 649) for 60 min. After washing three times with PBS, cells were added with 4,6-diamidino-2-phenylindole for nuclear counter-staining and mounted. Samples were analyzed, and fluorescence images were captured using a NIKON A1Si spectral detector confocal system equipped with ×40 (dry) lenses. ImageJ version 3.91 software was used to perform the image analysis (41).

Flow cytometry

J774A.1 cells were seeded onto 12-well plates (5×10^5 cells per well). Macrophage cell subpopulation marker iNOS was analyzed by flow cytometry to evaluate the M1 phenotype. After 24 h of culture, cells were stimulated by titanium particles for 24 h, then trypsinized, scraped from the plates, centrifuged, and resuspended in 1% BSA for 30 min at ambient temperature for blocking nonspecific antigens. Then the cells were incubated with phycoerythrin-conjugated iNOS (eBioscience) for 30 min at ambient temperature. After washing twice with PBS, cells were resuspended in 1% BSA and analyzed on FACSVerse™ (BD Biosciences). Data were analyzed using FACSuite software.

Mouse model of particle-induced osteolysis and bioluminescence imaging

8-Week-old C57BL/6J male mice were purchased from the Animal Laboratory of Sun Yat-sen University (Guangzhou, Guangdong, China) and raised for 2 weeks in a specific pathogen-free condition at the Laboratory Animal Center, Sun Yat-sen University (Guangzhou, Guangdong, China), so that all mice were 10 weeks of age and 18–20 g of weight for surgery. These mice were divided into four groups, with five mice in each group, and anesthetized by chloral hydrate via intraperitoneal injection. A 15-mm midline sagittal incision on the head of the mouse was made for the exposure of the calvarium. A 0.5×0.5-cm^2 gelatin sponge was placed over calvarium with periosteum scraped off for the continuous Ti particle infusion. Ti particles (0.3 mg of Ti particles suspended in 30 μl of PBS per mouse) and a murine reporter macrophage cell line J774A.1 transfected with different lentiviral vectors (0.5×10^6 cells suspended in 0.1 ml PBS per mouse) were injected in Ti + vector group, Ti + NLRC5-LV group, and Ti + USP14-LV group at the mid-line sagittal suture of the calvarium before suturing. A sham operation (a midline sagittal incision on the head of the mouse was made and 130 μl of PBS were injected before suturing) was taken as the blank control.

Murine reporter macrophages were injected at the mid-line sagittal suture of the calvarium to simulate the local infusion of macrophages in the presence of Ti particle stimulus. The murine macrophage cell line J774A.1 transfected with the lentiviral vector to express the bioluminescent optical reporter gene, firefly luciferase (fluc), was used as a reporter cell for local macrophage recruitment to the area of inflammation (42). PE IVIS Lumina $LT_{III\,S}$ (PerkinElmer Life Sciences) was used for *in vivo* BLI. Luciferase substrate D-luciferin was administered by intraperitoneal injection (3 mg/mouse). Ten minutes after substrate injection, vertical images were taken of the whole mouse. Mice were imaged immediately after macrophage injection (day 0) and then imaged every other day for 1 week (day 7). After imaging at day 7, mice were euthanized, and the calvaria were collected with all soft tissues obliterated for micro-CT imaging. Animal experiments were performed in accordance with the guidelines and approval of the Institutional Animal Care and Use Committee (IACUC) at Sun Yat-sen University (L102022018060E).

CT scan analysis and microcomputed tomography

The calvaria were fixed with formalin for 2 days after obtaining. Subsequently, the scan with a high-resolution *in vivo* micro-CT imaging system (ZKKS-MCT-Sharp, Japan) at 60 kV and 667 μA within 240 ms and the qualitative analysis in the associated software were performed. All projection frames were recorded five times and then averaged. 3D images were reconstructed with the associated manufacturer reconstruction software. The BMD, TV, BV, and BV/TV were measured from a $1 \times 3 \times 3$-mm ROI in cross-section slices around the sagittal suture.

Immunohistochemistry assay of mouse calvaria

Mouse calvaria obtained from four groups were fixed in formalin for 48 h and subsequently decalcified in 10% EDTA for 21 days, followed by embedding in paraffin wax for 4.0-μm serial sectioning. The sections were deparaffinized through xylene immersion, rehydrated by graded ethanol, and treated with 0.1% trypsin for 45 min at 37 °C. After blocking in 20% goat serum for 30 min at room temperature, the sections were hatched, respectively, with anti-mouse Trap mAb (1:100 diluted, Abcam), anti-mouse TNFα mAb (1:100 diluted, Abcam), and anti-mouse IL-6 mAb (1:100 diluted, Proteintech) at 37 °C for 2 h, followed by cultivation with horseradish peroxidase–conjugated secondary antibody (Zhongshanjinqiao Biotechnology, P.R., China) for 30 min at room temperature. DAB was used as chromogenic agent and hematoxylin as second staining. Finally, the samples were washed by water, dried, and affixed with neutral balsam, and then observed by a biomicroscope (DM2000, Leica, German). $Trap^+$ cell numbers were counted within an interested area. The interested area was defined using a magnification of ×10, as one microscope sight of the calvarial bone with the midline suture centered (43).

Statistics

SPSS 20.0 software package (Chicago, IL) was used for statistical analyses. Every result came from at least three independent experiments. Student's t test or one-way analysis of variance was employed to determine the statistical significance of the differences. The data were presented as the mean ± standard deviation. A value of $p < 0.05$ was regarded as statistically significant.

Author contributions—G. F., S. Li, J. Q., C. L., and Y. D. conceptualization; G. F., Y. F., J. Q., and S. Lin data curation; G. F., Y. F., and S. Lin software; G. F., Y. F., S. Li, J. Q., M. K., and S. Lin formal analysis; G. F., Y. F., and S. Lin investigation; G. F., Y. F., M. K., and S. Lin methodology; G. F. and Y. F. writing-original draft; G. F., S. Li, J. Q., C. L., and Y. D. writing-review and editing; S. Li, C. L., and Y. D. project administration; M. K. and Y. D. resources; C. L. and Y. D. funding acquisition; Y. D. supervision.

References

1. Man, K., Jiang, L., Foster R., and Yang, X. (2017) Immunological responses to total hip arthroplasty. *J. Funct. Biomater.* **8,** 33 CrossRef Medline
2. Sadoghi, P., Liebensteiner, M., Agreiter, M., Leithner, A., Böhler, N., and Labek, G. (2013) Revision surgery after total joint arthroplasty: a complication-based analysis using worldwide arthroplasty registers. *J. Arthroplasty* **28,** 1329–1332 CrossRef Medline
3. Jun, L. R., Ke, T., Long, K. B., Lin, Y. Y., Zhen-peng, G., Dian-ge, Z., and Jian-hao, L. (2018) Causes and management of revision hip arthroplasty. *Orthoped. J. China* **26,** 1729–1734
4. Massin, P., and Achour, S. (2017) Wear products of total hip arthroplasty: the case of polyethylene. *Morphologie* **101,** 1–8 CrossRef Medline
5. Pajarinen, J., Lin, T. H., Nabeshima, A., Jämsen, E., Lu, L., Nathan, K., Yao, Z., and Goodman, S. B. (2017) Mesenchymal stem cells in the aseptic loosening of total joint replacements. *J. Biomed. Mater. Res. A* **105,** 1195–1207 CrossRef Medline
6. Eger, M., Hiram-Bab, S., Liron, T., Sterer, N., Carmi, Y., Kohavi, D., and Gabet, Y. (2018) Mechanism and prevention of titanium particle–induced inflammation and osteolysis. *Front. Immunol.* **9,** 2963 CrossRef Medline
7. Yang, H., Xu, Y., Zhu, M., Gu, Y., Zhang, W., Shao, H., Wang, Y., Ping, Z., Hu, X., Wang, L., and Geng, D. (2016) Inhibition of titanium-particle-induced inflammatory osteolysis after local administration of dopamine and suppression of osteoclastogenesis via D2-like receptor signaling pathway. *Biomaterials* **80,** 1–10 CrossRef Medline
8. Murray, P. J., Allen, J. E., Biswas, S. K., Fisher, E. A., Gilroy, D. W., Goerdt, S., Gordon, S., Hamilton, J. A., Ivashkiv, L. B., Lawrence, T., Locati, M., Mantovani, A., Martinez, F. O., Mege, J. L., Mosser, D. M., *et al.* (2014) Macrophage activation and polarization: nomenclature and experimental guidelines. *Immunity* **41,** 14–20 CrossRef Medline
9. Gu, Q., Yang, H., and Shi, Q. (2017) Macrophages and bone inflammation. *J. Orthop. Transl.* **10,** 86–93 CrossRef
10. Wang, X., Li, Y., Feng, Y., Cheng, H., and Li, D. (2019) Macrophage polarization in aseptic bone resorption around dental implants induced by Ti particles in a murine model. *J. Periodontal Res.* **54,** 329–338 CrossRef Medline
11. Horwood, N. J. (2016) Macrophage polarization and bone formation: a review. *Clin. Rev. Allergy Immunol.* **51,** 79–86 CrossRef Medline
12. Li, B., Hu, Y., Zhao, Y., Cheng, M., Qin, H., Cheng, T., Wang, Q., Peng, X., and Zhang, X. (2017) Curcumin attenuates titanium particle–induced inflammation by regulating macrophage polarization *in vitro* and *in vivo*. *Front. Immunol.* **8,** 55 28197150
13. Lin, T. H., Tamaki, Y., Pajarinen, J., Waters, H. A., Woo, D. K., Yao, Z., and Goodman, S. B. (2014) Chronic inflammation in biomaterial-induced periprosthetic osteolysis: NF-κB as a therapeutic target. *Acta Biomater.* **10,** 1–10 CrossRef Medline
14. Holding, C. A., Findlay, D. M., Stamenkov, R., Neale, S. D., Lucas, H., Dharmapatni, A. S., Callary, S. A., Shrestha, K. R., Atkins, G. J., Howie, D. W., and Haynes, D. R. (2006) The correlation of RANK, RANKL and TNFα expression with bone loss volume and polyethylene wear debris around hip implants. *Biomaterials* **27,** 5212–5219 CrossRef Medline
15. An, S., Han, F., Hu, Y., Liu, Y., Li, J., and Wang, L. (2018) Curcumin inhibits polyethylene-induced osteolysis via repressing NF-κB signaling pathway activation. *Cell. Physiol. Biochem.* **50,** 1100–1112 CrossRef Medline
16. Feng, W., Li, J., Liao, S., Ma, S., Li, F., Zhong, C., Li, G., Wei, Y., Huang, H., Wei, Q., Yao, J., and Liu, Y. (2018) Gö6983 attenuates titanium particle–induced osteolysis and RANKL mediated osteoclastogenesis through the suppression of NFκB/JNK/p38 pathways. *Biochem. Biophys. Res. Commun.* **503,** 62–70 CrossRef Medline
17. Zhou, C. H., Shi, Z. L., Meng, J. H., Hu, B., Zhao, C. C., Yang, Y. T., Yu, W., Chen, Z. X., Heng, B. C., Parkman, V. A., Jiang, S., Zhu, H. X., Wu, H. B., Shen, W. L., and Yan, S. G. (2018) Sophocarpine attenuates wear particle–induced implant loosening by inhibiting osteoclastogenesis and bone resorption via suppression of the NF-κ B signalling pathway in a rat model. *Br. J. Pharmacol.* **175,** 859–876 CrossRef Medline
18. Huang, J. B., Ding, Y., Huang, D., Liang, A. J., Zeng, W. K., Zeng, Z. P., Qin, C. Q., and Barden, B. (2013) Inhibition of the PI3K/AKT pathway reduces tumor necrosis factor-α production in the cellular response to wear particles *in vitro*. *Artif. Organs* **37,** 298–307 CrossRef Medline
19. Huang, J. B., Ding, Y., Huang, D. S., Zeng, W. K., Guan, Z. P., and Zhang, M. L. (2013) RNA interference targeting p110β reduces tumor necrosis factor-α production in cellular response to wear particles *in vitro* and osteolysis *in vivo*. *Inflammation* **36,** 1041–1054 CrossRef Medline
20. Wu, L., Guo, Q., Yang, J., and Ni, B. (2017) Tumor necrosis factor α promotes osteoclast formation via PI3K/Akt pathway-mediated blimp1 expression upregulation. *J. Cell. Biochem.* **118,** 1308–1315 CrossRef Medline
21. Linton, M. F., Moslehi, J. J., and Babaev, V. R. (2019) Akt signaling in macrophage polarization, survival, and atherosclerosis. *Int. J. Mol. Sci.* **20,** E2703 CrossRef Medline
22. Benkö, S., Kovács, E. G., Hezel, F., and Kufer, T. A. (2017) NLRC5 functions beyond MHC I regulation–what do we know so far? *Front. Immunol.* **8,** 150 CrossRef Medline
23. Cui, J., Zhu, L., Xia, X., Wang, H. Y., Legras, X., Hong, J., Ji, J., Shen, P., Zheng, S., Chen, Z. J., and Wang, R. (2010) NLRC5 negatively regulates the NF-κB and type I interferon signaling pathways. *Cell* **141,** 483–496 CrossRef Medline
24. Tong, Y., Cui, J., Li, Q., Zou, J., Wang, H. Y., and Wang, R. (2012) Enhanced TLR-induced NF-κB signaling and type I interferon responses in NLRC5 deficient mice. *Cell Res.* **22,** 822–835 CrossRef Medline
25. Wang, M., Wang, L., Fang, L., Li, S., and Liu, R. (2019) NLRC5 negatively regulates LTA-induced inflammation via TLR2/NF-κB and participates in TLR2-mediated allergic airway inflammation. *J. Cell. Physiol.* CrossRef
26. Han, F., Gao, Y., Ding, C. G., Xia, X. X., Wang, Y. X., Xue, W. J., Ding, X. M., Zheng, J., and Tian, P. X. (2018) Knockdown of NLRC5 attenuates renal I/R injury *in vitro* through the activation of PI3K/Akt signaling pathway. *Biomed. Pharmacother.* **103,** 222–227 CrossRef Medline
27. Meng, Q., Cai, C., Sun, T., Wang, Q., Xie, W., Wang, R., and Cui, J. (2015) Reversible ubiquitination shapes NLRC5 function and modulates NF-κB activation switch. *J. Cell Biol.* **211,** 1025–1040 CrossRef Medline
28. Akira, S., Uematsu, S., and Takeuchi, O. (2006) Pathogen recognition and innate immunity. *Cell* **124,** 783–801 CrossRef Medline
29. Zhang, C., Li, C., Li, S., Qin, L., Luo, M., Fu, G., Qiu, J., Peng, P., Cai, W., and Ding, Y. (2018) Small heterodimer partner negatively regulates TLR4 signaling pathway of titanium particles-induced osteolysis in mice. *J. Biomed. Nanotechnol.* **14,** 609–618 CrossRef Medline
30. Negroni, A., Pierdomenico, M., Cucchiara, S., and Stronati, L. (2018) NOD2 and inflammation: current insights. *J. Inflamm. Res.* **11,** 49–60 CrossRef Medline
31. Vaden, J. H., Bhattacharyya, B. J., Chen, P. C., Watson, J. A., Marshall, A. G., Phillips, S. E., Wilson, J. A., King, G. D., Miller, R. J., and Wilson, S. M. (2015) Ubiquitin-specific protease 14 regulates c-Jun N-terminal kinase signaling at the neuromuscular junction. *Mol. Neurodegener.* **10,** 3 CrossRef Medline

32. Chelbi, S. T., Dang, A. T., and Guarda, G. (2017) Emerging major histocompatibility complex class I-related functions of NLRC5. *Adv. Immunol.* **133,** 89–119 CrossRef Medline
33. Benkö, S., Kovács, E. G., Hezel, F., and Kufer, T. A. (2017) NLRC5 functions beyond MHC I regulation—what do we know so far? *Front. Immunol.* **8,** 150 CrossRef Medline
34. Vijayan, S., Sidiq, T., Yousuf, S., van den Elsen. P. J., and Kobayashi, K. S. (2019) Class I transactivator, NLRC5: a central player in the MHC class I pathway and cancer immune surveillance. *Immunogenetics* **71,** 273–282 CrossRef Medline
35. Wang, S., Liu, R., Yu, Q., Dong, L., Bi, Y., and Liu, G. (2019) Metabolic reprogramming of macrophages during infections and cancer. *Cancer Lett.* **452,** 14–22 CrossRef Medline
36. Qi, W., Lin, C., Fan, K., Chen, Z., Liu, L., Feng, X., Zhang, H., Shao, Y., Fang, H., Zhao, C., Zhang, R., and Cai, D. (2019) Hesperidin inhibits synovial cell inflammation and macrophage polarization through suppression of the PI3K/AKT pathway in complete Freund's adjuvant-induced arthritis in mice. *Chem. Biol. Interact.* **306,** 19–28 CrossRef Medline
37. Li, S., Qiu, J., Qin, L., Peng, P., Li, C., Mao, J., Fang, G., Chen, Z., Lin, S., Fu, Y., Cai, W., and Ding, Y. (2019) NOD2 negatively regulated titanium particle–induced osteolysis in mice. *Biomater. Sci.* **7,** 2702–2715 CrossRef Medline
38. Mialki, R. K., Zhao, J., Wei, J., Mallampalli, D. F., and Zhao, Y. (2013) Overexpression of USP14 protease reduces I-κB protein levels and increases cytokine release in lung epithelial cells. *J. Biol. Chem.* **288,** 15437–15441 CrossRef Medline
39. Li, M., Zhao, J., and Jia, L. (2019) USP14-mediated IκBα degradation exacerbates NF-κB activation and IL-1β–stimulated chondrocyte dedifferentiation. *Life Sci.* **218,** 147–152 CrossRef Medline
40. Bresalier, R. S., Ho, S. B., Schoeppner, H. L., Kim, Y. S., Sleisenger, M. H., Brodt, P., and Byrd, J. C. (1996) Enhanced sialylation of mucin-associated carbohydrate structures in human colon cancer metastasis. *Gastroenterology* **110,** 1354–1367 CrossRef Medline
41. Noursadeghi, M., Tsang, J., Haustein, T., Miller, R. F., Chain, B. M., and Katz, D. R. (2008) Quantitative imaging assay for NF-κB nuclear translocation in primary human macrophages. *J. Immunol. Methods* **329,** 194–200 CrossRef Medline
42. Nabeshima, A., Pajarinen, J., Lin, T. H., Jiang, X., Gibon, E., Córdova, L. A., Loi, F., Lu, L., Jämsen, E., Egashira, K., Yang, F., Yao, Z., and Goodman, S. B. (2017) Mutant CCL2 protein coating mitigates wear particle–induced bone loss in a murine continuous polyethylene infusion model. *Biomaterials* **117,** 1–9 CrossRef Medline
43. von Knoch, M., Jewison, D. E., Sibonga, J. D., Turner, R. T., Morrey, B. F., Loer, F., Berry, D. J., and Scully, S. P. (2004) Decrease in particle-induced osteolysis in obese (ob/ob) mice. *Biomaterials* **25,** 4675–4681 CrossRef Medline